

Human Heme Oxygenase Oxidation of 5- and 15-Phenylhemes*

Received for publication, June 7, 2004, and in revised form, August 3, 2004
Published, JBC Papers in Press, August 5, 2004, DOI 10.1074/jbc.M406346200

Jinling Wang[‡], Fernando Niemevz[§], Latesh Lad[¶], Liusheng Huang[‡], Diego E. Alvarez[§],
Graciela Buldain[§], Thomas L. Poulos[¶], and Paul R. Ortiz de Montellano[‡]||

From the [‡]Department of Pharmaceutical Chemistry, University of California, San Francisco, California 94143-2280, the [¶]Department of Molecular Biology and Biochemistry, Department of Physiology and Biophysics, Department of Chemistry and Program in Macromolecular Structure, University of California, Irvine, California 92697-3900, and the [§]Departamento de Química Orgánica, Facultad de Farmacia y Bioquímica, Universidad de Buenos Aires, Junin 956 (C1113AAD), Buenos Aires, Argentina

Human heme oxygenase-1 (hHO-1) catalyzes the O₂-dependent oxidation of heme to biliverdin, CO, and free iron. Previous work indicated that electrophilic addition of the terminal oxygen of the ferric hydroperoxo complex to the α -meso-carbon gives 5-hydroxyheme. Earlier efforts to block this reaction with a 5-methyl substituent failed, as the reaction still gave biliverdin IX α . Surprisingly, a 15-methyl substituent caused exclusive cleavage at the γ -meso- rather than at the normal, unsubstituted α -meso-carbon. No CO was formed in these reactions, but the fragment cleaved from the porphyrin eluded identification. We report here that hHO-1 cleaves 5-phenylheme to biliverdin IX α and oxidizes 15-phenylheme at the α -meso position to give 10-phenylbiliverdin IX α . The fragment extruded in the oxidation of 5-phenylheme is benzoic acid, one oxygen of which comes from O₂ and the other from water. The 2.29- and 2.11-Å crystal structures of the hHO-1 complexes with 1- and 15-phenylheme, respectively, show clear electron density for both the 5- and 15-phenyl rings in both molecules of the asymmetric unit. The overall structure of 15-phenylheme-hHO-1 is similar to that of heme-hHO-1 except for small changes in distal residues 141–150 and in the proximal Lys¹⁸ and Lys²². In the 5-phenylheme-hHO-1 structure, the phenyl-substituted heme occupies the same position as heme in the heme-HO-1 complex but the 5-phenyl substituent disrupts the rigid hydrophobic wall of residues Met³⁴, Phe²¹⁴, and residues 26–42 near the α -meso carbon. The results provide independent support for an electrophilic oxidation mechanism and support a role for stereochemical control of the reaction regioselectivity.

Heme¹ oxygenase, the rate-limiting enzyme in the heme degradation pathway, oxidizes heme to biliverdin, carbon monoxide, and free iron (1) (Fig. 1). In humans and other mammals,

the heme is cleaved exclusively at the α -meso position to give biliverdin IX α . The biliverdin then is reduced to bilirubin by biliverdin reductase before it is conjugated with glucuronic acid and excreted in the bile (2). Bilirubin is a powerful physiological antioxidant (3), but is neurotoxic at the high concentrations found in Crigler Najar patients and neonatal jaundice (4). CO, the second product of the reaction, is a gaseous messenger molecule that is thought to be involved in apoptosis (5), atherosclerosis (6), psoriasis (7), vascular constriction (8), cellular protection (9), and chronic renal inflammation (10). Finally, the ferrous iron released by heme oxygenase is normally recycled and serves as the major source of this metal for hemoglobin and other hemoprotein synthesis, as only 1–3% of the iron utilized daily in the synthesis of red blood cells is obtained from the diet (11). Thus, in addition to its other functions, heme oxygenase plays a vital role in maintaining iron homeostasis.

In mammals, there are three heme oxygenase isoforms, namely HO-1, HO-2, and HO-3. HO-1 is inducible and present in highest concentration in spleen and liver. It is a stress protein also known as heat shock protein 32 that has been extensively studied because it is induced by a variety of agents, including heme, metals, hormones, oxidizing agents, and drugs (4, 12). Recently it was reported that HO-1 can prevent the inflammatory responses caused by adenovirus vectors in gene therapy (13). It is also a remarkably protective gene against allograft rejection (14, 15). HO-2 is constitutive and is found in highest concentration in the brain and testes. It may be involved in signaling pathways that involve CO and has been suggested to act as a nitric oxide sink (16), although this latter role remains controversial. HO-3 is also expressed constitutively, but it is a poor catalyst, and its role, if any, is unclear (17).

The mammalian heme oxygenases are membrane bound. However, a truncated human HO-1 construct (265 amino acids, hHO-1) lacking the 23 C-terminal amino acids is fully active and is water soluble (18). The successful expression of this truncated hHO-1 in *Escherichia coli* has greatly facilitated the molecular level characterization of hHO-1.

The mechanism of heme oxidation by heme oxygenase has been partially elucidated (19). Heme is converted to biliverdin IX α via two observable intermediates, 5-hydroxyheme and α -verdoheme (Fig. 1). Oxidation of heme to 5-hydroxyheme and of verdoheme to iron biliverdin requires NADPH-P450 reductase and O₂. The intervening step in which 5-hydroxyheme is converted to verdoheme only requires O₂ and results in the

* This work was supported by National Institutes of Health Grants DK30297 (to P. R. O. de M.) and GM33688 (to T. L. P.) and by Grant B0-26 (to G. B.) from the Universidad de Buenos Aires. The costs of publication of this article were defrayed in part by the payment of page charges. This article must therefore be hereby marked "advertisement" in accordance with 18 U.S.C. Section 1734 solely to indicate this fact.

The atomic coordinates and structure factors (codes 1S13 and 1T5P) have been deposited in the Protein Data Bank, Research Collaboratory for Structural Bioinformatics, Rutgers University, New Brunswick, NJ (<http://www.rcsb.org/>).

|| To whom correspondence should be addressed: University of California, San Francisco, Genentech Hall, 600 16th St., N572D, San Francisco, CA 94143-2280. Tel.: 415-476-2903; Fax: 415-502-4728; E-mail: ortiz@cgl.ucsf.edu.

¹ The abbreviations used are: heme, iron protoporphyrin IX regardless of oxidation and ligation state; hHO-1, wild-type human heme oxygenase-1; heme-hHO-1, complex of iron protoporphyrin IX with

hHO-1; 5-hHO-1, complex of 5-phenylheme with hHO-1; 15-hHO-1, complex of 15-phenylheme with hHO-1; 5-phenylheme, α -meso-phenylheme; 15-phenylheme, γ -meso-phenylheme; P450 reductase, NADPH-cytochrome P450 reductase; biliverdin reductase, biliverdin IX α reductase; Mb, horse myoglobin; LC-MS, liquid chromatography-mass spectrometry; r.m.s.d., root mean square deviation.

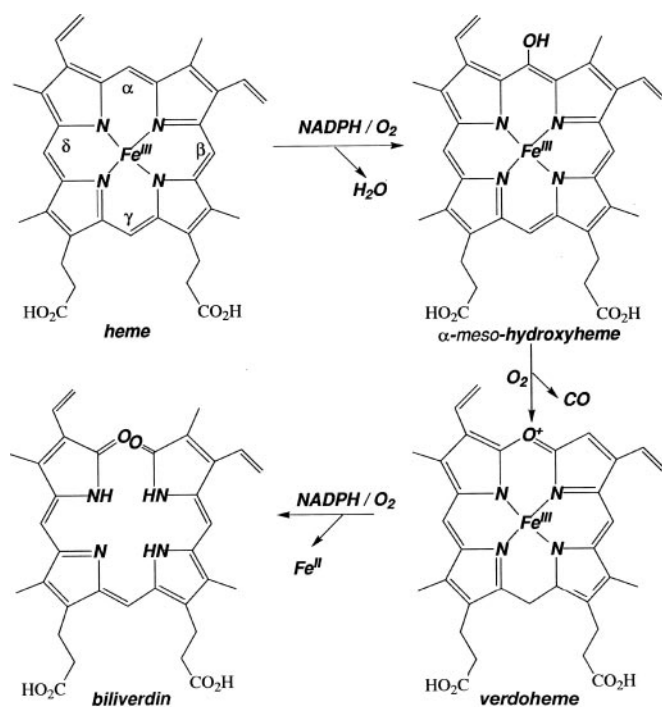


FIG. 1. Scheme of the oxidation of heme catalyzed by heme oxygenase. The α - (5-), β -, γ - (15-), and δ -*meso* positions of the heme are labeled.

release of CO. The degradation of heme by heme oxygenase is highly regiospecific. In mammals, heme is exclusively cleaved at the α -*meso* position to give biliverdin IX α (20, 21). However, the heme oxygenase from *Pseudomonas aeruginosa* oxidizes heme to biliverdin IX β and IX δ (22).

Torpey *et al.* (23) attempted in 1996 to use 5-methylmesoheme to block 5-hydroxylation and thus to inhibit the heme oxygenase reaction. Surprisingly, this compound was itself oxidized to biliverdin IX α , albeit without the formation of CO. Equally surprising was the finding that 15-methylmesoheme was exclusively cleaved at the γ position despite the presence of the normally oxidized, unsubstituted α position. Unfortunately it was not possible in these earlier studies to identify the product containing the methyl group and the α - or γ -*meso*-carbon atom. Nevertheless, the fact that CO was not formed clearly established that this unexpected oxidation did not involve initial removal of the methyl group from the *meso*-methylheme to give heme itself, which then underwent normal cleavage.

To further characterize the mechanism governing the degradation of the *meso*-substituted heme, we have now examined the hHO-1-catalyzed oxidation of the 5- and 15-phenylhemes (Fig. 2). A phenyl substituent was employed for these studies because its chromophore would facilitate identification and isolation of the fragment containing the *meso*-substituent and the *meso*-carbon atom. This assumes, of course, that the phenyl-substituted hemes are bound and are oxidized by hHO-1. In fact, we report here that 5-phenylheme is oxidized at the α -*meso* position to give biliverdin IX α with the concomitant release of benzoic acid. In contrast, unlike 15-methylheme, 15-phenylheme is exclusively cleaved at the normal α -*meso* position. The crystal structures of the 5- and 15-phenylheme complexes with hHO-1 have also been determined to clarify the structural perturbations caused by the phenyl substituent. The results clarify the mechanism of the heme cleavage and the origin of the reaction regiospecificity.

EXPERIMENTAL PROCEDURES

Materials—5-Phenylheme, 15-phenylheme, and the biliverdin isomers derived from the dimethyl esters of 5-phenylheme and 15-phenylheme (Fig. 2) were prepared as reported previously (24–26). The dimethyl-esterified biliverdin isomers were generated by published procedures (27). $^{18}O_2$ and $H_2^{18}O$ were from ICON Isotopes (Summit, NJ). Ampicillin, NADPH, Mb, sodium ascorbate, trifluoroacetic acid, and sodium dithionite were purchased from Sigma or Aldrich. Quaternary ammonium cellulose (QA52) was from Whatman Inc. BL21 (DE3) plysS-competent cells were obtained from Stratagene (La Jolla, CA). Methanol (HPLC grade) was from Fisher Scientific, the YMCTM ODS-AQ C18 column (S-5, 120 Å, 4.6 × 250 mm) was from Walters Corp., and the Sephadex G-50 quick spin column was from Roche Applied Science.

Enzymes—A truncated human heme oxygenase 1 (hHO-1) retaining amino acids 1–265 but lacking the 23 C-terminal amino acids was used in this study (18). Expression and purification were carried out as reported previously except that QA52 resin was used instead of the Q-Sepharose fast flow resin from Amersham Biosciences (28). The apo-hHO-1 was combined with excess heme, 5-phenylheme, or 15-phenylheme. The reconstituted hHO-1 (heme-hHO-1, 5-hHO-1, 15-hHO-1, respectively) was purified by passage through an Amersham Biosciences PD-10 desalting column pre-equilibrated with 0.1 M potassium phosphate buffer, pH 7.4 (defined here as the standard buffer). Human P450 reductase and rat biliverdin reductase were expressed and purified by published procedures (29–31). Superoxide dismutase and bovine liver catalase were from Sigma.

UV-visible Spectra of Heme-hHO-1, 5-hHO-1, and 15-hHO-1—The spectra were recorded in standard buffer at room temperature on a Cary Varian model 1E spectrophotometer.

Spectrophotometric Monitoring of Bilirubin Formation Using P450 Reductase and Biliverdin Reductase—The reaction mixture contained 6 μ g of heme-hHO-1, 4 μ M rat biliverdin reductase, 0.4 μ M P450 reductase, and 30 μ M heme in a final reaction volume of 100 μ l. Bilirubin formation was initiated by the addition of NADPH (400 μ M). The formation of bilirubin was monitored at 468 nm at 30-s intervals. For 5-phenylheme, the reaction mixture contained 5-hHO-1 and 5-phenylheme, and for 15-phenylheme, 15-hHO-1 and 15-phenylheme. All the reactions were performed at room temperature in standard buffer.

Spectrophotometric Monitoring of Fe(III) Biliverdin Formation Using Sodium Ascorbate—Heme-hHO-1, 5-hHO-1, or 15-hHO-1 (10 μ M) was incubated at room temperature with sodium ascorbate (3 mM) in 200 μ l of standard buffer for 1.5 h. The solution was then passed through a Sephadex G-50 quick spin column pre-equilibrated with standard buffer, and the UV-visible spectrum was recorded.

CO Formation Assay Using Horse Deoxymyoglobin as a CO Trap—Heme-hHO-1, 5-hHO-1, or 15-hHO-1 (10 μ M) in 1 ml of standard buffer was incubated in air tight vials at room temperature for 10 min with NADPH (400 μ M) and P450 reductase (1 μ M). Fe(II) Mb (50 μ l, 83 μ M) was then added to the solution via a syringe to a final concentration of 4 μ M. The solution was shaken well, and the UV-visible spectrum was recorded. The Fe(II) Mb (83 μ M) was freshly prepared by adding sodium dithionite solution (70 μ l, 1 M) to a metMb solution (350 μ l, 100 μ M) without further purification.

HPLC Analysis of Biliverdin Isomers—Heme-hHO-1, 5-hHO-1, or 15-hHO-1 (45 nmol) was incubated with NADPH (3.4 μ mol) and P450 reductase (4.5 nmol) in standard buffer for 2 h at room temperature. The reaction volume was 650 μ l. The reaction mixture turned reddish in the case of 5-hHO-1 and green in the case of heme-hHO-1 and 15-hHO-1. Methanol was added to a final concentration of 60%, and the resulting mixture was subjected to centrifugation. To the supernatant was added 1 drop of concentrated HCl plus a few drops of acetic acid before the solution was extracted with an equal volume of CH_2Cl_2 . The organic phase was washed with an equal volume of water and was then evaporated under a stream of air. The residual products were dissolved in methanol/5% H_2SO_4 (v/v), and the mixture was allowed to stand at room temperature for at least 16 h. The resulting dimethyl-esterified products were extracted with $CHCl_3$ and washed with water. The organic phase was dried under a stream of air, and the residue was dissolved in methanol. Before loading onto a YMCTM ODS-AQ C18 column, the concentration of methanol was adjusted to 60–70%.

Coupled oxidation with sodium ascorbate was carried out by incubating each of the complexes, *i.e.* heme-hHO-1, 15-hHO-1, or 5-hHO-1 (45 nmol), with sodium ascorbate (13 mg) in standard buffer for 2 h at room temperature. The reaction volume was ~320 μ l. The degradation products went through the same procedures as above for HPLC analysis.

The dimethyl-esterified products were loaded onto a YMCTM

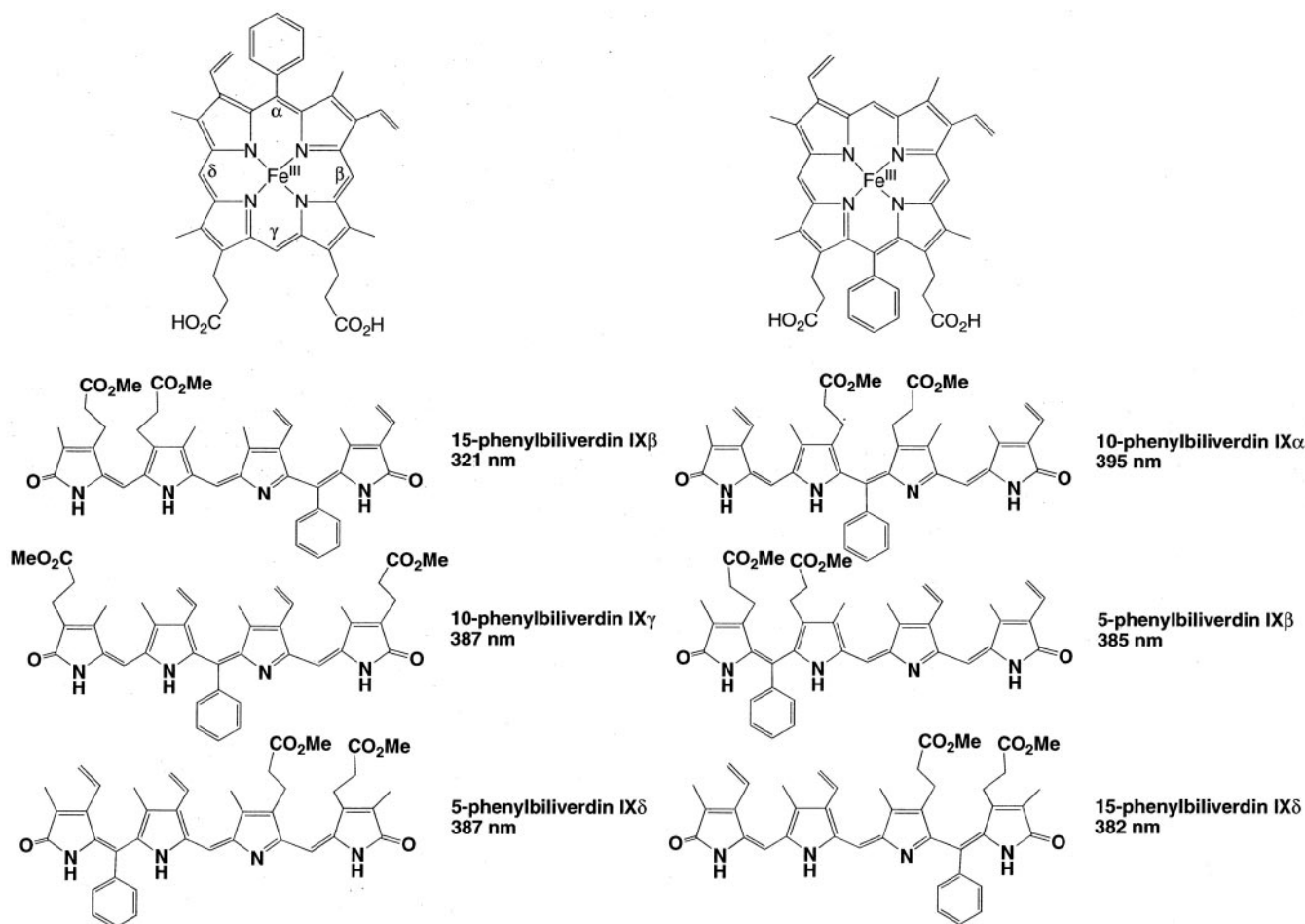


FIG. 2. *Left*, structures of 5-phenylheme and the phenyl-substituted biliverdin IX β , IX γ , and IX δ derived by coupled oxidation of the dimethyl ester of 5-phenylheme. *Right*, structures of 15-phenylheme and the phenyl-substituted biliverdin IX α , IX β , and IX δ isomers obtained by coupled oxidation of the dimethyl ester of 15-phenylheme (24–26). The electronic absorption maximum of each compound in CH_2Cl_2 is indicated.

ODS-AQ C18 column. HPLC was done with a Varian 1090 solvent delivery system and a Hewlett-Packard 1040A detector at room temperature. Solvents A and B were H_2O and methanol, respectively. The running conditions were the following: flow rate, 1.0 ml/min; 30% B for 5 min, 30–70% B in 0.1 min, 70–95% B in 25 min, 95% B for 10 min, 95–30% B in 5 min, and finally 30% B for 20 min. The eluent was monitored at 380 nm and referenced against 598 nm.

HPLC Analysis of the Fragment Containing the α -Carbon and Phenyl Group—The heme-hHO-1, 5-hHO-1, or 15-hHO-1 complex (~ 7 nmol) was incubated with NADPH (400 nmol) and P450 reductase (0.6 nmol) in standard buffer at room temperature for at least 1 h. Methanol and trichloroacetic acid were then added to the reaction solution to final concentrations of 60 and 10%, respectively. The resulting solution stood on ice for at least 30 min. The precipitate was removed by centrifugation, and the supernatant was loaded onto a YMC ODS-AQTM C18 column. HPLC was carried out at room temperature with a Varian 1090 solvent delivery system and a Hewlett-Packard 1040A detector, using the following conditions (solution A, $\text{H}_2\text{O}/0.05\%$ trifluoroacetic acid; solution B, methanol/0.1% trifluoroacetic acid, flow rate, 1.0 ml/min): 10% B for 5 min, 10–30% B in 0.1 min, 30–55% B in 25 min, 55–95% B in 5 min, 95% B for 5 min, 95–10% B in 0.1 min, and 10% B for 15 min. Benzoic acid and benzaldehyde standards were dissolved in a mixture of standard buffer, 60% methanol, 10% trichloroacetic acid. The eluent was monitored at 230 and 254 nm and was referenced against the absorption at 598 nm. Benzoic acid has a maximum absorption at 230 nm and benzaldehyde at 254 nm.

The incubation of 5-hHO-1 with P450 reductase and NADPH was also performed in the presence of superoxide dismutase and catalase. The reaction went through the same experimental protocol as above.

Mass Spectrometric Analysis of the Species Containing the α -Carbon and Phenyl Group—5-hHO-1 or heme-hHO-1 (29 nmol) was incubated with P450 reductase (2.9 nmol) and NADPH (1.8 μmol) at room temperature for 2 h. The final reaction volume was 116 μl . The reaction

mixture was injected into a Waters Micromass ZQ Mass Spectrometer. The equipment was run under electrospray ionization in negative ion mode (ES⁻ mode), and the mass spectra were analyzed using the MassLynxTM 3.5 program. The mass spectrum of 5-hHO-1 alone was also obtained as a control.

Origin of the Oxygen Atoms in the Benzoic Acid from Oxidation of 5-Phenylheme—Oxidation of 5-phenylheme by hHO-1 was carried out in either $^{18}\text{O}_2$ or H_2^{18}O . For the reaction in $^{18}\text{O}_2$, 5-hHO-1 (10 μl , 2.95 mM) and P450 reductase (5.8 μl , 274 μM) were added to 100 μl of standard buffer on the bottom of a two-necked flask. One drop of NADPH (30 μl , 0.1 M) was spotted separately on the inner wall. Air was removed by three cycles of purging with argon gas and placing under vacuum. NADPH was then mixed with the enzymes by shaking the flask slightly followed by introduction of $^{18}\text{O}_2$ into the flask. The mixture was allowed to stand at room temperature for 0.5 h before it was passed through an ultracentrifugal filter device (10,000 molecular weight cutoff, Millipore Amicon®) to remove the protein before analysis by liquid chromatography-mass spectrometry (LC-MS). For the reaction in H_2^{18}O , a mixture of 5-hHO-1 (5.4 μl , 2.95 mM) and P450 reductase (2.9 μl , 274 μM) was lyophilized for 1 h, dissolved in 50 μl of H_2^{18}O , and relyophilized for 1 h. The residue was dissolved in 100 μl of H_2^{18}O and was then mixed with 4 μl of NADPH (1 M in H_2^{18}O). The mixture was allowed to stand at room temperature for 0.5 h before it was passed through the ultracentrifugal filter device to remove the protein before analysis by LC-MS.

LC-MS was performed on a Waters Micromass ZQ coupled to a Waters Alliance HPLC system (2695 Separations Module, Waters 2487 Dual λ Absorbance detector) employing an Xterra[®] MS C18 column (2.1 \times 50 mm, 3.5 μm). For the chromatography, solvent A was 0.1% ammonium hydroxide in water and solvent B was methanol. The column was eluted with 5% solvent B (95% solvent A) at a flow rate of 0.2 ml/min. The eluent was monitored at 230 nm. The MS settings were: mode, ES⁻; capillary voltage, 2.9 kv; cone voltage, 20 v; source temperature, 130 $^\circ\text{C}$; desolvation temperature, 300 $^\circ\text{C}$. Masses

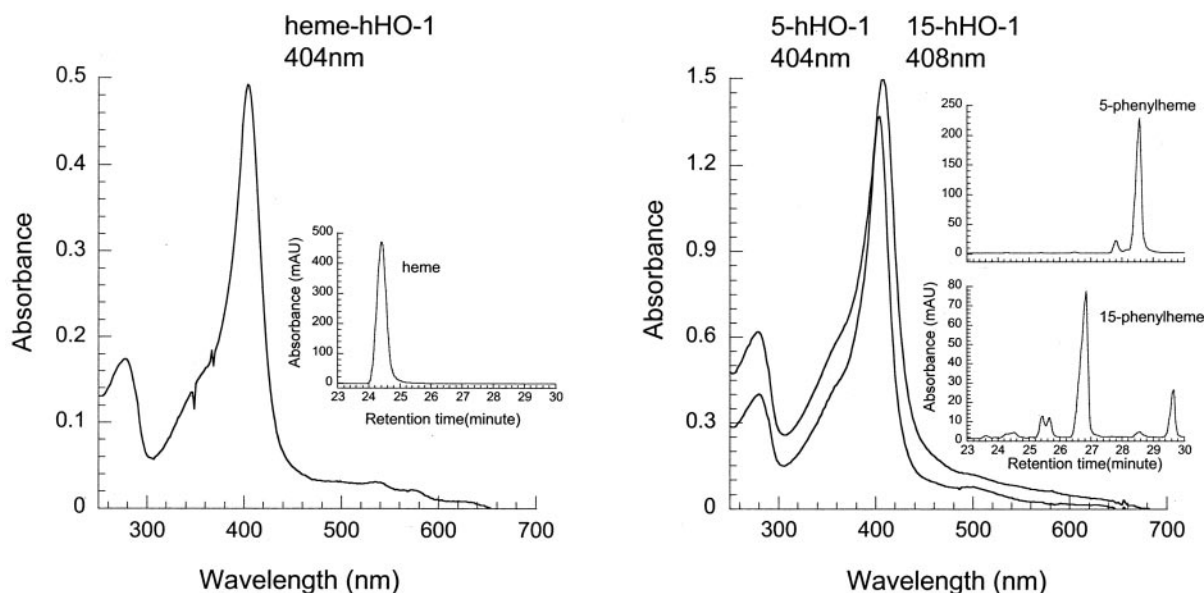


FIG. 3. UV-vis spectra of the complexes of hHO-1 with heme (heme-hHO-1), 5-phenylheme (5-hHO-1), and 15-phenylheme (15-hHO-1). The position of the Soret absorption maximum is indicated. The insets show the HPLC traces of heme, 5-phenylheme, and 15-phenylheme, respectively.

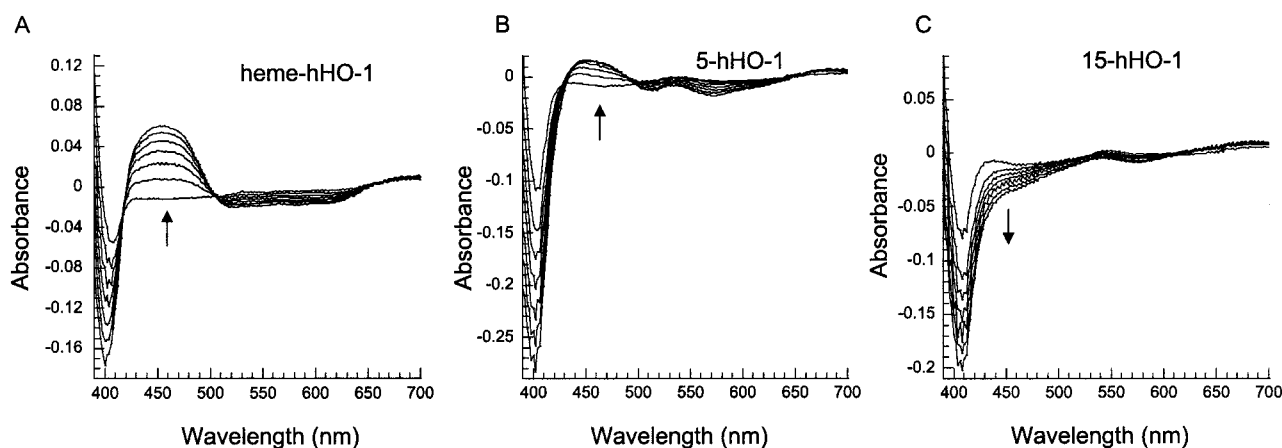


FIG. 4. Spectrophotometric monitoring of bilirubin formation in the presence of P450 reductase and biliverdin reductase. The spectra were monitored at 30-s intervals for 3 min. Bilirubin has an absorption maximum at 468 nm. The arrows indicate the direction of the time-dependent spectral change.

115–200 were scanned with a scan time of 0.2 s. The control experiment was performed by incubation of 5-hHO-1 (29 nmol) with P450 reductase (2.9 nmol) and NADPH (1.8 μ mol) in 100 μ l of standard buffer for 0.5 h.

Crystallography—Crystals of 15-hHO-1 and 5-hHO-1 were grown under slightly different conditions than those described previously (32, 33). Crystals were obtained using the hanging-drop vapor diffusion method with a well solution of 2.0–1.5 M ammonium sulfate, 100 mM HEPES, pH 7.5, 0.9% 1,6-hexanediol, and 10–30% Jeffamine ED-600. Drops consisted of protein stock (5 μ l) at 65 mg ml⁻¹ in 100 mM potassium phosphate, pH 7.4, mixed with well solution (5 μ l). Crystals were grown at room temperature, and one round of touch seeding using crushed wild-type crystals was necessary to initiate 15-hHO-1 crystal growth. For 5-hHO-1 macro seeding had to be used to obtain crystals of suitable size for data collection. For cryogenic data collection D-(+)-trehalose was used as the cryoprotectant. Cryogenic data collection involved a seven-step transfer to artificial precipitant solution with increased D-(+)-trehalose concentration up to 35% (w/v). Heme-hHO-1 and 5-hHO-1 crystals belong to the monoclinic space group, P2₁, whereas 15-hHO-1 crystals belong to the orthorhombic space group, P2₁2₁2₁. Cell dimensions of all the crystal forms are listed in Table I. Data were collected using an R-Axis IV imaging plate detector equipped with a rotating copper anode x-ray generator with Osmic optics (Rigaku). For this data set, a 180° scan using 1° frames was collected. Crystals were maintained at -160 °C in a stream of nitrogen (Crystal Logic, Los Angeles). Data were reduced

using HKL 2000 (34), and rejections were performed with ENDHKL (Louis Sanchez, California Institute of Technology) in conjunction with SCALEPACK.

Both the 15-hHO-1 and 5-hHO-1 structures were determined by the method of molecular replacement using AmoRe (35). A monomer of the human heme-hHO-1 crystal structure (Protein Data Bank accession number 1N45) (36), with the heme and waters removed, was used as the probe with searches carried out at 5 Å in either P2₁2₁2₁ (15-hHO-1) or P2₁ (5-hHO-1) space group. The best cross-rotation and translation function solutions were rigid body-refined and fixed in place followed by a search for the remaining molecule in the asymmetric unit. A total of two solutions was found per structure, corresponding to the expected two monomers per asymmetric unit. The final R-factors were 38 and 42% with correlation coefficients of 63 and 52% for 15-hHO-1 and 5-hHO-1, respectively. The structures were further refined in CNS (37). The structures were initially refined by simulated annealing, followed by a few cycles of conjugate gradient minimization and water picking. Finally, temperature factors were refined. No restraints for non-crystallographic symmetry were applied. The program O (38) was used for further adjustment and modeling of protein atoms, ligands, and water molecules. Backbone geometry was checked with PROCHECK (39), and none of the residues were in the disallowed region.

Data collection and refinement statistics are summarized in Table I, and the Protein Data Bank coordinates have been deposited in the Protein Data Bank (accession codes 1S13 and 1T5P).

RESULTS

UV-visible Spectra of Heme-hHO-1, 5-hHO-1, and 15-hHO-1—Apo-hHO-1 was combined with heme, 5-phenylheme, or 15-phenylheme and the resulting reconstituted heme oxygenase was immediately purified. The UV-visible spectra of the three reconstituted complexes (Fig. 3) show that both heme-hHO-1

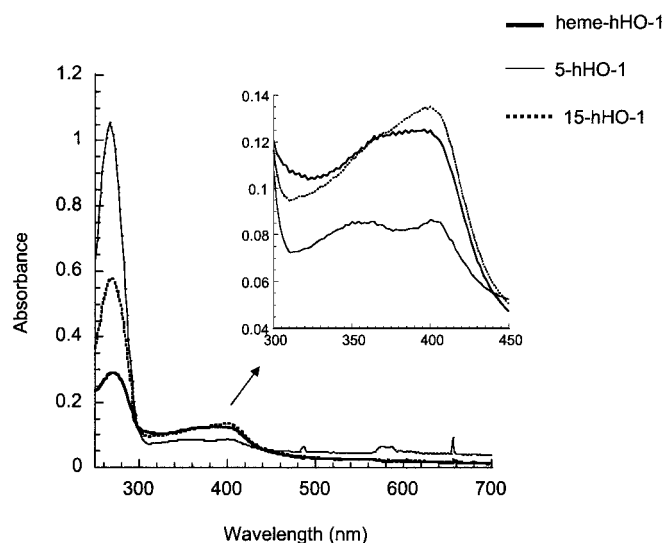


FIG. 5. **Fe(III) biliverdin formation under coupled oxidation conditions.** The complex (heme-hHO-1, 5-hHO-1, or 15-hHO-1) was incubated with sodium ascorbate for 2 h. The solution was then passed through a G-50 quick spin column, and the UV-visible spectrum was recorded.

and 5-hHO-1 have a Soret absorption maximum at 404 nm, whereas the maximum of the 15-hHO-1 complex is at 408 nm. As the Soret maxima in phosphate buffer at pH 7.4 of free heme, 5-phenylheme, and 15-phenylheme are at 364, 388, and 388 nm, respectively, there is a differential shift in the Soret maxima when they are bound in the hHO-1 active site. The shift for 5-phenylheme is 4 nm less than for 15-phenylheme, and both of the phenylhemes undergo a smaller shift than heme itself. These results confirm that the *meso*-phenyl hemes are able to bind to hHO-1 and suggest that their binding causes some perturbation of the active site.

Bilirubin and CO Formation Using P450 Reductase and Biliverdin Reductase—The normal degradation of heme by hHO-1 gives biliverdin IX α and CO. The electrons required for the degradation of heme are provided by NADPH via P450 reductase. Biliverdin IX α is then reduced to bilirubin IX α by biliverdin reductase. As shown in Fig. 4A, these combined reactions cause a decrease in the heme Soret absorption at 404 nm and the accumulation of bilirubin with an absorption maximum at 468 nm. For 5-phenylheme, the reaction gives very similar UV-visible spectral changes (Fig. 4B), *i.e.* a decrease in the Soret band intensity associated with an increase in absorption at 468 nm. For 15-phenylheme, however, the UV-visible spectral changes are different in that the absorption of both the Soret band at 408 nm and at 468 nm decreases (Fig. 4C).

The high affinity of Fe(II) Mb for CO has been used previously to detect CO formation in the oxidation of heme by hHO-1 (23), as the Soret absorption maximum at 434 nm of Fe(II) Mb shifts to 422 nm when CO is bound. Furthermore, the extinction coefficient of Fe(II)-CO Mb ($207 \text{ mM}^{-1} \text{ cm}^{-1}$) is ~ 2 -fold higher than that of Fe(II) Mb ($121 \text{ mM}^{-1} \text{ cm}^{-1}$) (40), which

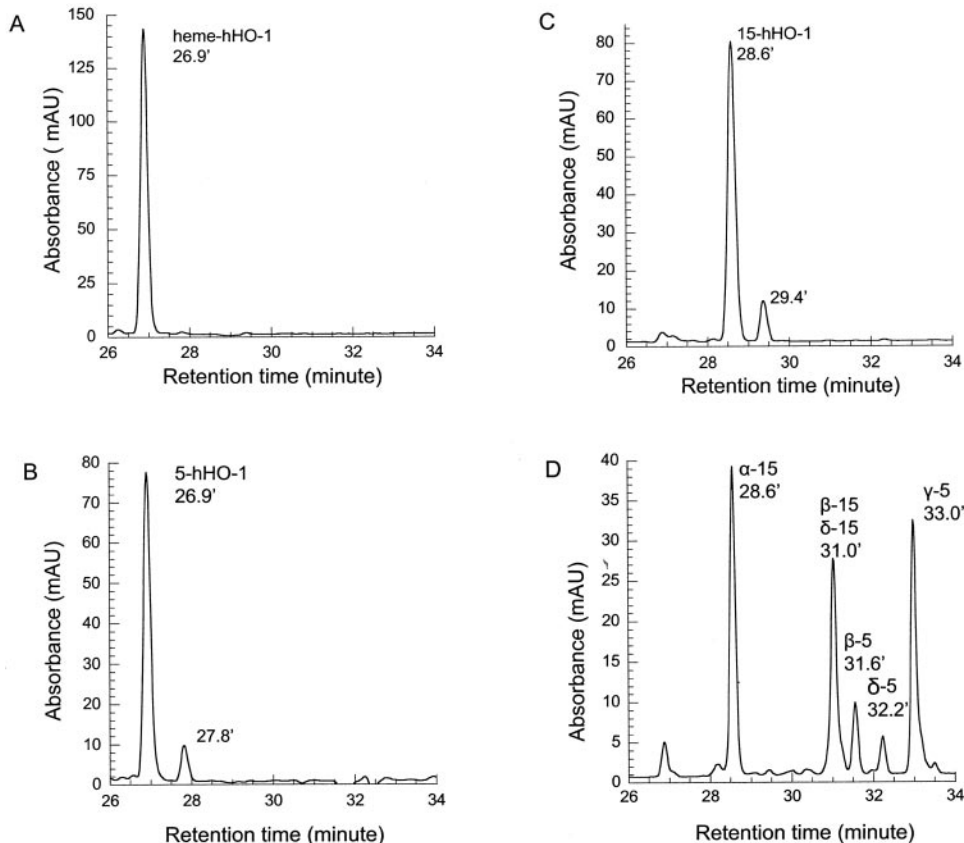


FIG. 6. HPLC analysis of the biliverdin dimethyl esters isolated from the reactions of the heme-hHO-1 (A), 5-hHO-1 (B), and 15-hHO-1 (C) complexes supported by NADPH-P450 reductase. A mixture of the standards obtained by coupled oxidation of 5-phenylheme and 15-phenylheme is shown in D, along with the assignments of the peaks based on the NMR structural analysis (24–26). The peaks are labeled as follows: β -5, 15-phenylbiliverdin IX β ; γ -5, 10-phenylbiliverdin IX γ ; δ -5, 5-phenylbiliverdin IX δ ; α -15, 10-phenylbiliverdin IX α ; β -15, 5-phenylbiliverdin IX β ; δ -15, 15-phenylbiliverdin IX δ .

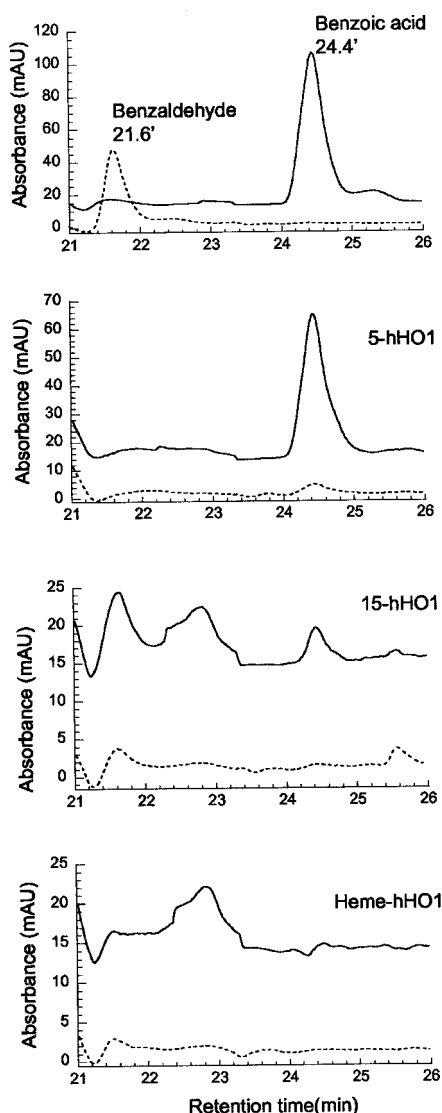


FIG. 7. HPLC analysis of the product containing the phenyl group and α -*meso*-carbon. The solid line is the absorbance at 230 nm, and the dashed line is the absorbance at 254 nm.

enhances the sensitivity of the assay. The reactions of heme-hHO-1, 5-hHO-1, or 15-hHO-1 with P450 reductase and NADPH were carried out in sealed vials. After completion of the reactions, Fe(II) Mb was injected into the vials. The Fe(II)-CO Mb complex was immediately formed if it was present. To make sure that all the Fe(II) Mb that was added bound CO, which improved the accuracy of the assay, a substoichiometric amount (0.4 equivalent) of Fe(II) Mb was used. The results of this assay indicate that both heme-hHO-1 and 15-hHO-1 produce CO (data not shown), whereas 5-hHO-1 does not. In view of the spectrophotometric demonstration of bilirubin formation (Fig. 4), it is clear that hHO-1 catalyzes the degradation of the two phenyl-substituted hemes. 5-Phenylheme is cleaved at the α position, as no CO is released, whereas 15-phenylheme is cleaved at a position other than the γ -*meso* position, probably at the normal α -*meso* position, resulting in the formation of CO.

Fe(III) Biliverdin Formation Using Sodium Ascorbate—The degradation of heme by hHO-1 to Fe(III) biliverdin can be supported by the surrogate electron donor sodium ascorbate. Fig. 5 shows that incubation of 5-hHO-1 with ascorbate gives a spectrum with a broad absorption at around 380 nm similar to

that obtained by coupled oxidation of heme-hHO-1. This spectrum corresponds to that of the hHO-1 complex of ferric biliverdin IX α . However, the spectrum obtained on coupled oxidation of 15-hHO-1 has a maximum of absorption at 400 nm and is quite different. This result is consistent with the already described bilirubin and CO formation studies, all of which suggest that 5-phenylheme is degraded enzymatically by hHO-1 without CO release, probably to biliverdin IX α . In contrast, the oxidation of 15-phenylheme by hHO-1 yields CO and one or more products thought to be phenyl-substituted biliverdins.

HPLC Analysis of Biliverdin Isomers—To simplify the identification of biliverdin isomers by HPLC, all the biliverdin isomers produced by coupled oxidation of heme, 5-phenylheme, and 15-phenylheme were converted to the corresponding dimethyl esters. The coupled oxidation was carried out in the absence of hHO-1 and thus gave mixtures of the isomers expected from cleavage at each of the three non-phenyl substituted *meso* positions in each molecule (Fig. 2) (24–26). As shown in Fig. 6A, incubation of heme-hHO-1 with NADPH-P450 reductase gives a single HPLC peak that corresponds to the dimethyl ester of biliverdin IX α (λ_{\max} = 375 nm, retention time = 26.9 min). The HPLC conditions employed here (see “Experimental Procedures”) separate the isomeric biliverdin dimethyl esters very well except for the dimethyl esters of 5-phenylbiliverdin IX β and 15-phenylbiliverdin IX δ , both of which have a retention time of 31.0 min (Fig. 6D). Incubation of 5-hHO-1 with NADPH-P450 reductase produces a species with exactly the same retention time and spectrum as the dimethyl ester of biliverdin IX α (Fig. 6B). In the case of 15-hHO-1, the product has a retention time (28.6 min) and spectrum (λ_{\max} = 393 nm) that correspond to the dimethyl ester of 10-phenylbiliverdin IX α (Fig. 6C). It is thus clear that both phenyl-substituted hemes are cleaved at the α position. A minor product peak is also observed in the HPLC traces for 5-hHO-1 and 15-hHO-1 (Fig. 6, B and C), but these peaks do not co-elute with the dimethyl esters of the α -, β -, γ -, or δ -biliverdin isomers (data not shown). The identities of these minor products are therefore obscure, although they may derive from the minor impurities present in the original 5- and 15-phenylheme samples (Fig. 3).

The same products as were obtained in the reactions supported by P450 reductase are obtained in the ascorbate-supported degradation of heme and the phenyl-substituted compounds by hHO-1, *i.e.* biliverdin IX α and 10-phenylbiliverdin IX α (data not shown). Among other things, this establishes that the heme oxidations occurred entirely within the hHO-1 complex and not in solution, as a mixture of the isomers is obtained in solution. Interestingly, coupled oxidation with ascorbate of the 5- and 15-phenylhemes in the absence of the enzyme results in oxidation of only the three non-substituted *meso* positions (Fig. 2) (25, 26). Thus, the observation that the phenyl-substituted position of the 5-hHO-1 complex is exclusively oxidized, whether the reaction is supported by NADPH-P450 reductase or ascorbate, clearly demonstrates that the stereochemical control imposed by the enzyme overrides the inherent higher reactivity of the unsubstituted *meso* positions.

Identification of the Product Containing the α -*meso*-Carbon and Phenyl Group—The results above clearly establish that 5-phenylheme is oxidized by hHO-1 to biliverdin IX α . What, then, is the identity of the product that contains the α -*meso*-carbon and the phenyl group attached to it? The most obvious possibilities are benzaldehyde and benzoic acid, although other products can be envisioned. Under our HPLC conditions (see “Experimental Procedures”) authentic benzoic acid elutes at 24.4 min and benzaldehyde at 21.6 min. Not only are the two

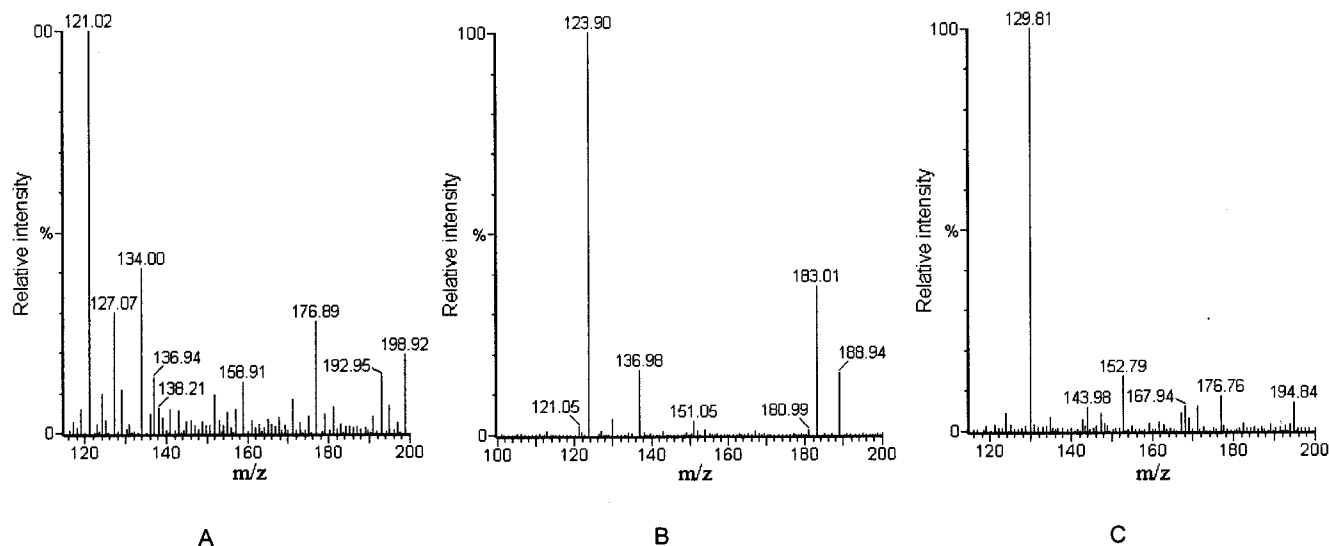


FIG. 8. Mass spectrum of the reaction mixture of 5-hHO-1 + P450 reductase + NADPH (A), heme-hHO-1 + P450 reductase + NADPH (B), and 5-hHO-1 alone (C). The ion intensities for the peaks at m/z 121.02 (A), 123.90 (B), and 129.81 (C) are 1.2×10^6 , 1.1×10^5 , and 6.2×10^3 , respectively. The sensitivity in B and C was set much higher than in A to determine whether any signal was present at m/z 121.

molecules well separated, but benzoic acid has an absorption maximum at 230 nm and benzaldehyde at 254 nm. The two are therefore readily distinguished. Incubation of 5-hHO-1 with NADPH-P450 reductase produces a peak with the same retention time and absorption spectrum as benzoic acid but no detectable benzaldehyde (Fig. 7). However, as benzaldehyde is susceptible to oxidation and could have been a precursor of the observed benzoic acid, we repeated the experiment in the presence of superoxide dismutase and catalase. Again, only benzoic acid was detected. As a further control, we allowed a solution of benzaldehyde to stand at room temperature for several days and then analyzed the solution by HPLC. No benzoic acid was detected. These control experiments confirm that the initial product in the reaction is benzoic acid and not benzaldehyde. In the incubations of 15-hHO-1 with P450 reductase, a trace amount of what appears to be benzoic acid was detected. Close inspection of the products found in the P450 reductase-supported reaction (Fig. 6C) shows traces of products that might correspond to biliverdin IX γ , but repeated analysis rules this out. The trace amount of benzoic acid detected in Fig. 7 in the 15-hHO-1 plot therefore must derive from the impurities in the original sample (Fig. 3), as no benzoic acid is generated in control incubations of heme-hHO-1 with P450 reductase (Fig. 7).

Mass spectra of the reaction mixtures from incubations of 5-hHO-1 with NADPH-P450 reductase were obtained in the ES $^-$ mode (Fig. 8). An ion of m/z 121.02, which corresponds to the expected molecular ion of benzoic acid (molecular weight 122.04), was detected (Fig. 8A). To rule out the possibility that the benzoic acid detected was due to contamination from any of the three reaction constituents (5-hHO-1, P450 reductase, and NADPH), two controls were carried out. One was to incubate heme-hHO-1 with P450 reductase and NADPH, then to take the mass spectrum of the reaction mixture. The second control was to obtain the mass spectrum of 5-hHO-1 alone. No benzoic acid was detected in these control experiments (Fig. 8, B and C).

To identify the origin of the oxygen atoms in the benzoic acid, the reaction of 5-hHO-1 with P450 reductase and NADPH was performed in $^{18}\text{O}_2$ and H_2^{18}O , respectively, followed by LC-MS analysis. For the reaction in normal water under a normal atmosphere of air, a species with the same retention time as authentic benzoic acid (1.9 min) and the expected mass of 121

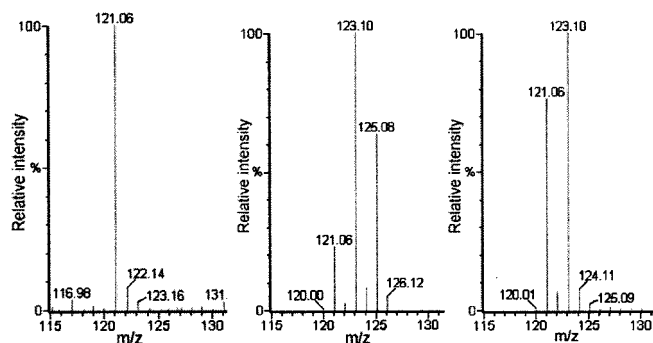


FIG. 9. Molecular ion region of the mass spectra of benzoic acid isolated from a normal incubation (left) and incubations carried out in $^{18}\text{O}_2$ (middle) and H_2^{18}O (right).

(m/z) under ES $^-$ mode was observed (Fig. 9, left). In contrast, singly ^{18}O -labeled benzoic acid with a mass of 123 (m/z) was detected in the reaction performed in H_2^{18}O . The ratio of unlabeled and single labeled benzoic acid is about 1.0:1.3 (Fig. 9, right). For the reaction carried out in $^{18}\text{O}_2$, however, both singly and doubly ^{18}O -labeled benzoic acid with masses of 123 (m/z) and 125 (m/z), respectively, were observed (Fig. 9, middle). The ratio of unlabeled, singly labeled, and doubly labeled benzoic acid is about 1.0:4.5:3.0. These results suggest that one oxygen atom in benzoic acid comes from oxygen gas and the other from water. Since the heme oxygenase reaction generates water within the active site, the reaction in $^{18}\text{O}_2$ can, as found, give rise to some incorporation of a second atom of ^{18}O through addition of *in situ* generated labeled water.

15-hHO-1 and 5-hHO-1 Structures—Both 15-hHO-1 and 5-hHO-1 complexes crystallized under slightly different conditions than the heme-hHO-1 complex, in that the addition of Jeffamem ED-600 was required to obtain suitable crystals. The final *R*-factors for the refined structures were 21.4 and 24.3% for 15-hHO-1 and 5-hHO-1, respectively (Table I).

Fig. 10 shows an omit electron density map of the 15-phenylheme in 15-hHO-1. The phenyl group is well defined, but only one of the heme propionates is visible. The apparently disordered propionate was omitted from the model. The 15-phenylheme is flatter than the heme in heme-hHO-1 and does

TABLE I
Data collection and refinement statistics

Values in parentheses are for the outermost shell.

	15hHO-1	5h-HO-1
Protein Data Bank code	1S13	1T5P
Crystal data		
Radiation source	$R_{\text{axis-IV}}$	$R_{\text{axis-IV}}$
Space group	$P2_12_12_1$	$P2_1$
Cell parameters (Å) and β (°)	$a = 55.0, b = 75.75$ $c = 107.3, \beta = 90.00$	$a = 52.91, b = 64.43$ $c = 60.47, \beta = 90.02$
Data collection		
Detector distance (nm)	140	140
Molecules per asymmetric unit	2	2
Resolution (Å)	2.29	2.11
Mosaicity (°)	0.67	1.1
Total observations	241,896	308,112
Unique reflections	49,102	62,102
Completeness (%)	99.9	91.8
Mean I/σ	11.5 (2.1)	10.1 (2.0)
R_{sym} (%)	5.1 (46.7)	5.4 (49.3)
Refinement statistics ^a		
R_{cryst}	0.22	0.25
R_{free}	0.25	0.29
r.m.s.d. bond lengths (Å) ^b	0.006	0.006
r.m.s.d. angles (°) ^b	1.1	1.2
Water molecules	185	109
Ramachandran angles		
Most favored (%)	94.9	96.3
Additional allowed (%)	5.1	3.7

^a $R_{\text{cryst}} = \sum(|F_{\text{obs}}| - |F_{\text{calc}}|) / \sum |F_{\text{obs}}|$. The R_{free} is the R_{cryst} calculated on the 5% reflections excluded for refinement.

^b r.m.s. bond and r.m.s. angle represent the root mean square deviation between the observed and ideal values.

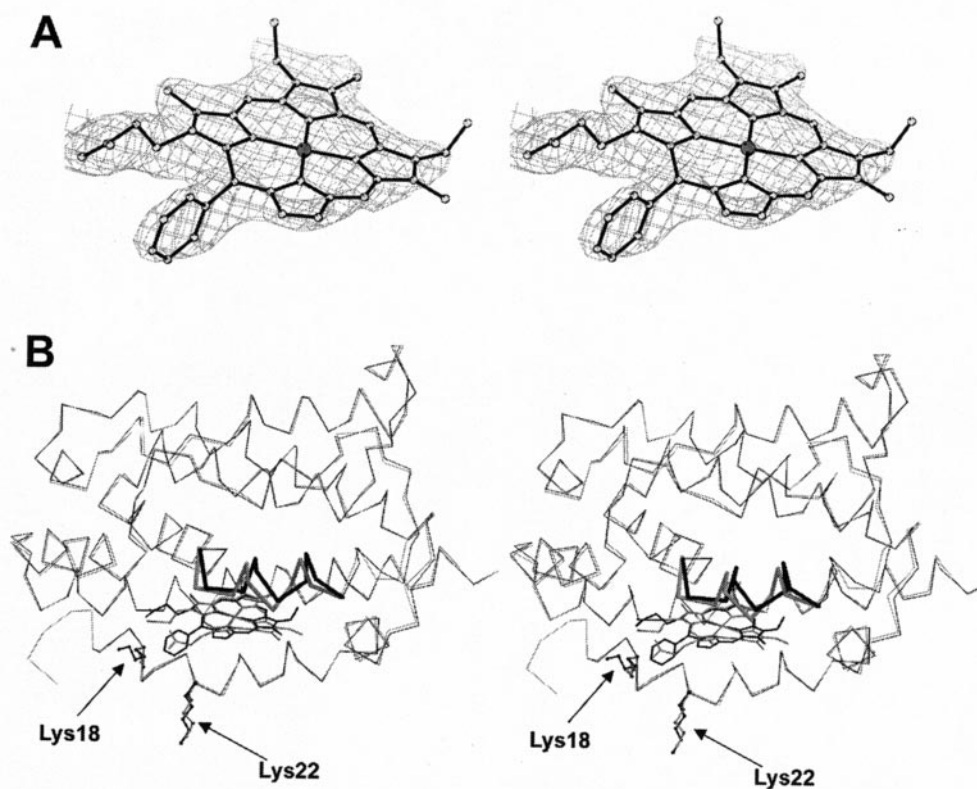


FIG. 10. **Crystal structure of 15-hHO-1.** *A*, stereo diagram of the $2F_o - F_c$ omit electron density contoured at 1σ around 15-phenylheme of 15-hHO-1. *B*, stereo view comparison of the backbone atoms between heme-hHO-1 (gray) and 15-hHO-1 (black). Thick lines represent regions of substantial change between the two sets of structures. The proximal residues Lys¹⁸ and Lys²² are also shown.

not have a distal water ligand. The overall structures of 15-hHO-1 and heme-hHO-1 are the same with a root mean square deviation (r.m.s.d.) of only 0.38 Å. However, a closer analysis of the heme active site reveals subtle differences caused by the need to accommodate the 15-phenyl substituent (Fig. 10*B*). These differences are confined to parts of the distal helix,

residues 141–150 (Fig. 10*B*, thick lines), and Lys¹⁸ and Lys²² of the proximal helix (Fig. 10*B*). The stretch of residues in the distal helix from residue 141 to 150 shifts ~ 1.2 Å inward (away from the bulk solvent) in the 15-hHO-1 versus heme-hHO-1 structure. On the proximal side Lys¹⁸ and Lys²², which in heme-hHO-1 stabilize the outer heme propionate group, move

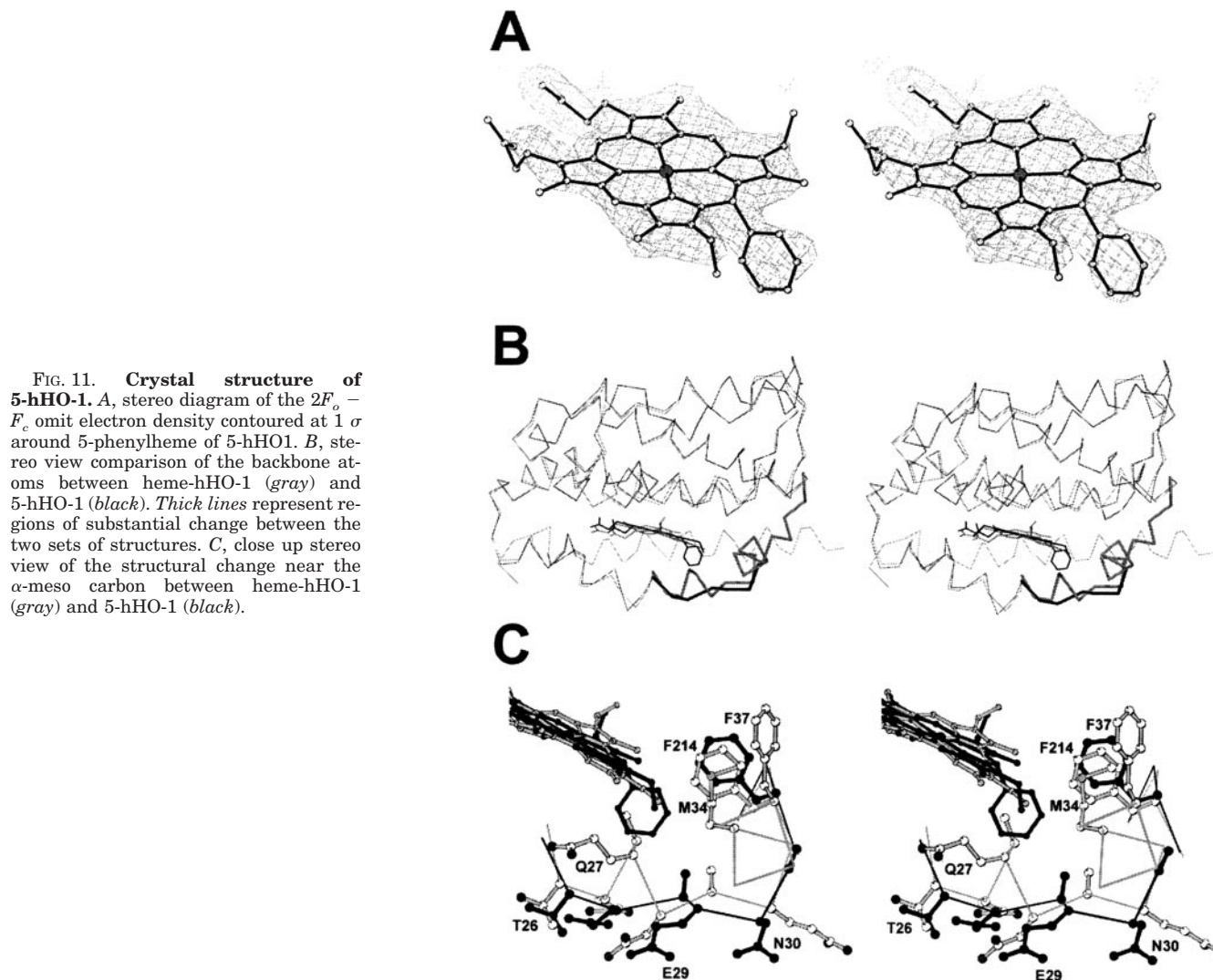


FIG. 11. **Crystal structure of 5-hHO-1.** A, stereo diagram of the $2F_o - F_c$ omit electron density contoured at 1σ around 5-phenylheme of 5-hHO-1. B, stereo view comparison of the backbone atoms between heme-hHO-1 (gray) and 5-hHO-1 (black). Thick lines represent regions of substantial change between the two sets of structures. C, close up stereo view of the structural change near the α -meso carbon between heme-hHO-1 (gray) and 5-hHO-1 (black).

away in the 15-hHO-1 structure. These changes in the distal and proximal helices are required to accommodate the heme 15-phenyl ring in 15-hHO-1. Most importantly, the orientation of the 15-phenylheme remains unchanged, leaving the α -meso heme carbon in exactly the same position as that in the heme-hHO-1 complex. This, together with the lack of changes in key catalytic groups such as Asp¹⁴⁰, explains why the 15-phenylheme is hydroxylated at the same α -meso carbon as the unsubstituted heme.

Fig. 11A shows an omit electron density map of the 5-phenylheme in 5-hHO-1. As in the case of 15-hHO-1, the overall structure of 5-phenylheme is flat, no distal water ligand is observed, and the phenyl group points down from the heme plane. However, in the 5-hHO-1 structure both heme propionate groups are visible, and the distal helix, including key catalytic residues such as Asp¹⁴⁰, remains relatively unchanged in comparison to the heme-hHO-1 structure (Fig. 11B). The major difference between the heme-hHO-1 and 5-hHO-1 structures is in the immediate vicinity of the α -meso heme carbon (Fig. 11, B and C). In the heme-hHO-1 structure the α -meso position faces a wall of hydrophobic residues including Met³⁴, Phe³⁷, and Phe²¹⁴ that remains unperturbed when ligands bind or when the heme is replaced by biliverdin IX α or verdoheme (36, 41–44). However, in the 5-hHO-1 structure electron density for Met³⁴, Phe³⁷, and residues 32–42 is not visible and, hence, must be disordered. A close comparison of the α -meso carbon region between the heme-hHO-1 and

5-hHO-1 structures reveals that the 5-phenyl ring would clash with Gln²⁷ (Fig. 11C). As a result Gln²⁷ and residues 28–31 must move to accommodate the 5-phenyl substituent on the heme (Fig. 11C). In the 5-hHO-1 structure the backbone atoms of Gln²⁷ must flip by 180° to avoid steric clashes with the phenyl ring. As a consequence residues 32–42 must also move but apparently do not adopt a new fixed conformation, since these residues now are disordered. Thus, the protein adapts to the new phenyl group by a disordering of the interior hydrophobic structure, which then allows the modified heme to adopt the same orientation as that observed in the heme HO-1 structure. This helps to explain why oxidation still occurs at the α -meso carbon.

DISCUSSION

Hydroxylation of heme to 5-hydroxyheme is the first step in the conversion of heme to biliverdin by mammalian heme oxygenases. The mechanism of this reaction has been proposed to involve electrophilic addition of the terminal oxygen in the ferric hydroperoxo complex to the α -meso-carbon, followed by elimination of the *meso*-proton to give the 5-hydroxyheme product (45). The evidence for this mechanism comes from observation of the ferric hydroperoxo complex in cryogenic experiments (46), from the demonstration that reaction of heme-hHO-1 with ethylhydroperoxide gives the 5-ethoxyheme product (47) and from the observation that an electron donating *meso*-methyl substituent favors, and an electron withdrawing substituent

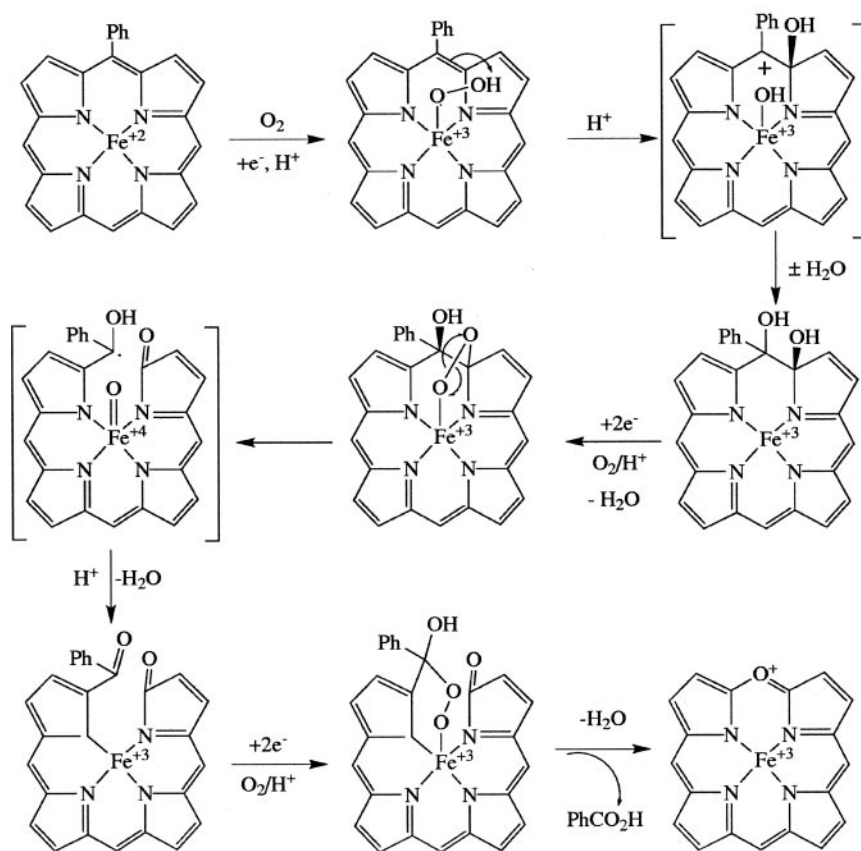


FIG. 12. Scheme showing one possible mechanism for the oxidation of 5-phenylheme to biliverdin IX α and benzoic acid that accounts for the observed incorporation of one oxygen from O₂ and one from H₂O.

disfavors, reaction at the substituted *meso*-carbon (23, 48). Furthermore, mechanistic studies indicate that the *meso*-hydroxy group is critical for the second step of the reaction sequence, the conversion of 5-hydroxyheme to verdoheme. Thus, EPR studies in the presence and absence of CO, used in the experiment to trap the iron in the ferrous state, show that electron transfer from the *meso*-hydroxyl reduces the iron and produces a carbon radical that reacts with molecular oxygen to set up the carbon-carbon bond cleavage reaction (49).

Substitution of the α -*meso* position with a methyl or phenyl group prevents formation of 5-hydroxyheme. This is confirmed by the fact that the oxidation does not yield CO and therefore does not proceed via the normal oxidation sequence (23). It is therefore necessary to postulate an oxidation mechanism that diverges from that for the normal oxidation but still produces the same biliverdin product (even if not CO). The present finding that the hHO-1-catalyzed oxidation of 5-phenylheme yields benzoic acid (Fig. 7) narrows the possibilities for this alternative mechanism. By inference, this result suggests that the group eliminated in the oxidation of 5-methylheme is acetic acid (23). The bond between the α -*meso*-carbon and the attached substituent therefore remains intact in the reaction, in accord with the failure to form CO. Control experiments establish that the benzoic acid is the immediate product and does not result from autoxidation of benzaldehyde. The reaction requires two oxidative steps and the introduction of two oxygen atoms, one of which is presumably the oxygen from the ferric hydroperoxy intermediate normally involved in the reaction.

Although the mechanistic scope for the oxidation of 5-phenylheme by hHO-1 is defined by the present studies, the actual mechanism for the reaction remains elusive. It is difficult to postulate a mechanism for the reaction that does not involve an additional intermediate. Thus, one possibility is electrophilic addition of the ferric hydroperoxy species to give an epoxide or, after water addition, a diol intermediate (Fig. 12). This inter-

mediate could then be converted to biliverdin IX α and benzoic acid in a second oxidative step. Further detailed analysis of the reaction is required to see if such an intermediate can be detected and characterized.

The oxidation of 15-phenylheme by hHO-1 occurs at the normal α -*meso* position to give 10-phenylbiliverdin IX α and CO. HPLC analysis confirms that the reaction yields exclusively the 10-phenylbiliverdin IX α isomer expected from cleavage at the α -*meso* position. In a sense, this is the least surprising site for the reaction, given that the oxidation occurs at all, because it is the site normally oxidized by the enzyme. However, it is unexpected because our earlier work showed that the 15-methylheme was oxidized not at the normal α -*meso* position but at the unnatural, substituted γ -*meso*-carbon (23). To determine whether the 15-substituent perturbed the active site structure in a manner that explained the different regiochemistries of 15-methyl *versus* 15-phenyl oxidation, we have determined the structure of the complexes of hHO-1 with both 5- and 15-phenylheme. Surprisingly, the substituted heme structure, if anything, is flatter than that of the more distorted heme normally bound in the hHO-1 active site (Figs. 10 and 11). Although *meso* substitution is commonly associated with puckering of the heme ring (50–52), AM1 calculations predict that the porphyrin ring in 15-phenylprotoporphyrin IX will be flat, whereas that in the 5-phenyl isomer will be distorted into a saddle shape (24). The 15-phenyl ring, which is predicted and found to be non-coplanar with the porphyrin ring, is accommodated by a shift of residues 141–150 by 1.2 Å and by displacement of Lys¹⁸ and Lys²². The shift of the helix includes residue Asp¹⁴⁰, which is involved in a hydrogen-bonding network that includes the distal water residue and is thought to be involved in activation of the iron-bound dioxygen molecule (53, 54). These changes are associated with an increased disorder in the position of the heme propionic acid group that normally interacts with Lys¹⁸ and Lys²². As a result, the propionic acid group

is not seen in the electron density map.

Despite the modest structural changes, the surprising result is that the 15-phenyl causes only a modest perturbation of the active site. As it appears unlikely that a *meso*-methyl will perturb the active site to a greater extent than a *meso*-phenyl, the stereochemical difference must be controlled by other factors. A methyl substituent ($\sigma = -0.37$ to -0.10) is considerably more electron donating than a phenyl group ($\sigma = -0.07$ to 0.22) (55), which would favor electrophilic addition to the methyl-substituted but not phenyl-substituted position relative to the normally oxidized unsubstituted α -*meso*-carbon. This difference in electronic effects probably contributes to the divergent oxidation regiochemistries observed with the *meso*-methyl and *meso*-phenyl substituents, but we cannot rule out the possibility that subtle structural changes are important.

The changes in the distal helix observed in 15-hHO-1 do not occur in the 5-hHO-1 structure but instead unexpectedly large changes are observed in the vicinity of the α -*meso* carbon (Fig. 11B). In the heme-HO-1 structure the α -*meso*-carbon faces a wall of hydrophobic residues, Met³⁴, Phe³⁷, and Phe²¹⁴, which are generally considered to be quite rigidly held in place. However, introduction of the 5-phenyl ring causes a major disruption in this hydrophobic wall. Electron density for Met³⁴ and Phe³⁷ is absent, suggesting a disordering of these residues, which most likely correlates with the 180° flip of Glu²⁷ to avoid collision with the 5-phenyl ring (Fig. 11C). Although residues 32–42 are disordered in the 5-hHO-1 structure, other nearby residues (residues 26–31) are visible and clearly have moved to accommodate the 5-phenyl ring (Fig. 11C). The ability of the hydrophobic wall to accommodate the heme phenyl ring thus enables the modified heme to adopt the same orientation as is observed in the heme-hHO-1 complex. The propionates remain oriented toward the surface, where they interact with charged groups. That the heme-propionate interactions remain unchanged, while the hydrophobic wall near the α -*meso* edge disorders indicates that the heme-propionate interactions must be very important in properly orienting the heme. The importance of propionate-protein interactions is supported by mutagenesis studies (56). Furthermore, the recently determined crystal structure of a bacterial heme oxygenase from *P. aeruginosa*, a HO enzyme that primarily hydroxylates the δ -*meso*-carbon, shows that the novel regioselectivity is due to rotation of the heme by $\sim 100^\circ$ (57). The rotation of the heme was primarily due the stabilizing contacts of the heme propionates in one orientation *versus* the other. The 5-hHO-1 structure provides further evidence that heme propionate-protein interactions play a key role in orienting the heme for proper regioselective hydroxylation.

The present results have identified the fragment lost from 5-phenylheme as benzoic acid, which implicates the existence of at least one additional reaction intermediate in the unusual oxidation of 5-substituted hemes by heme oxygenase. Structural data on the enzyme complexes of 5-phenylheme and 15-phenylheme shows that the 15-phenyl is readily accommodated with only minor structural perturbation of the active site, whereas one wall of the active site is dismantled to accommodate the 5-phenyl group. Interestingly, despite the structural changes that cause loss of the distal water ligand, both complexes are catalytically active and result in processing of the *meso*-substituted hemes.

REFERENCES

- Tenhunen, R., Marver, H. S., and Schmid, R. (1969) *J. Biol. Chem.* **244**, 6388–6394
- Schmid, R., and McDonagh, A. F. (1979) in *The Porphyrins* (Dolphin, D., ed) Vol. VI, pp. 257–292, Academic Press, New York
- Stocker, R., Yamamoto, Y., McDonagh, A. F., Glazer, A. N., and Ames, B. N. (1987) *Science* **235**, 1043–1046
- Maines, M. D. (1992) *Heme Oxygenase: Clinical Applications and Functions*, CRC Press, Boca Raton, FL
- Sass, G., Soares, M. C., Yamashita, K., Seyfried, S., Zimmermann, W. H., Eschenhagen, T., Kaczmarek, E., Ritter, T., Volk, H. D., and Tiegs, G. (2003) *Hepatology* **38**, 909–918
- Ishikawa, K., Sugawara, D., Wang, X., Suzuki, K., Itabe, H., Maruyama, Y., and Lusic, A. (2001) *Circ. Res.* **88**, 506–512
- Hanselmann, C., Mauch, C., and Werner, S. (2001) *Biochem. J.* **353**, 459–466
- Duckers, H. J., Boehm, M., True, A. L., Yet, S.-F., San, H., Park, J. L., Webb, R. C., Lee, M.-E., Nabel, G. J., and Nabel, E. G. (2001) *Nat. Med.* **7**, 693–698
- Clark, J. E., Foresti, R., Green, C. J., and Motterlini, R. (2000) *Biochem. J.* **348**, 615–619
- Nath, K. A., Vercellotti, G. M., Grande, J. P., Miyoshi, H., Paya, C. V., Manivel, J. C., Haggard, J. J., Croatt, A. J., Payne, W. D., and Alam, J. (2001) *Kidney Int.* **59**, 106–117
- Uzel, C., and Conrad, M. E. (1998) *Semin. Hematol.* **35**, 27–34
- Choi, A. M., and Alam, J. (1996) *Am. J. Respir. Cell Mol. Biol.* **15**, 9–19
- McCarter, S. D., Scott, J. R., Lee, P. J., Zhang, X., Choi, A. M., McLean, C. A., Badhwar, A., Dungey, A. A., Bihari, N. H., Harris, K. A., and Potter, R. F. (2003) *Gene Ther.* **10**, 1629–1635
- Soares, M. P., Brouard, S., Smith, R. N., and Bach, F. H. (2001) *Immunol. Rev.* **184**, 275–285
- Visner, G. A., Lu, F., Zhou, H., Latham, C., Agarwal, A., and Zander, D. S. (2003) *Transplantation* **76**, 650–656
- Ding, Y., McCoubrey, W. K., Jr., and Maines, M. D. (1999) *Eur. J. Biochem.* **264**, 854–861
- McCoubrey, W. K., Jr., Huang, T. J., and Maines, M. D. (1997) *Eur. J. Biochem.* **247**, 725–732
- Wilks, A., Black, S. M., Miller, W. L., and Ortiz de Montellano, P. R. (1995) *Biochemistry* **34**, 4421–4427
- Auclair, K., and Ortiz de Montellano, P. R. (2002) in *Porphyrin Handbook* (Kadish, K., Smith, K., and Guillard, R., eds) Vol. 12, pp. 183–210, Academic Press, New York
- Tenhunen, R., Marver, H. S., and Schmid, R. (1968) *Proc. Natl. Acad. Sci. U. S. A.* **61**, 748–755
- O'Carra, P. (1975) in *Porphyrins and Metalloporphyrins* (Smith, K. M., ed) pp. 123–153, Elsevier Sciences B. V., Amsterdam
- Ratliff, M., Zhu, W., Deshmukh, R., Wilks, A., and Stojiljkovic, I. (2001) *J. Bacteriol.* **183**, 6394–6403
- Torpey, J., and Ortiz de Montellano, P. R. (1996) *J. Biol. Chem.* **271**, 26067–26073
- Robinson, A. E., Maier, M. S., and Buldain, G. Y. (2000) *Heterocycles* **53**, 2127–2142
- Niemevez, F., Alvarez, D. E., and Buldain, G. Y. (2002) *Heterocycles* **57**, 697–704
- Niemevez, F., and Buldain, G. Y. (2004) *J. Porphyrins Phthalocyanines*, in press
- Crusats, J., Suzuki, A., Mizutani, T., and Ogoshi, H. (1998) *J. Org. Chem.* **63**, 602–607
- Wilks, A., Medzhradszky, K. F., and Ortiz de Montellano, P. R. (1998) *Biochemistry* **37**, 2889–2896
- Shen, A. L., Christensen, M. J., and Kasper, C. B. (1991) *J. Biol. Chem.* **266**, 19976–19980
- Liu, Y., and Ortiz de Montellano, P. R. (2000) *J. Biol. Chem.* **275**, 5297–5307
- Lightning, L. K., Huang, H., Moenne-Loccoz, P., Loehr, T. M., Schuller, D. J., Poulos, T. L., and Ortiz de Montellano, P. R. (2001) *J. Biol. Chem.* **276**, 10612–10619
- Schuller, D. J., Wilks, A., Ortiz de Montellano, P. R., and Poulos, T. L. (1998) *Protein Sci.* **7**, 1836–1838
- Schuller, D. J., Wilks, A., Ortiz de Montellano, P. R., and Poulos, T. (1999) *Nat. Struct. Biol.* **6**, 860–867
- Otwinowski, Z., and Minor, W. (1997) *Methods Enzymol.* **276**, 307–326
- Navaza, J. (1994) *Acta Crystallogr. Sect. A* **50**, 157–163
- Lad, L., Schuller, D. J., Shimizu, H., Friedman, J., Li, H., Ortiz de Montellano, P. R., and Poulos, T. L. (2003) *J. Biol. Chem.* **278**, 7834–7843
- Brünger, A. T., Adams, P. D., Clore, G. M., DeLano, W. L., Gros, P., Grosse-Kunstleve, R. W., Jiang, J.-S., Kuszewski, J., Nilges, M., Pannu, N. S., Read, R. J., Rice, L. M., Simonson, T., and Warren, G. L. (1998) *Acta Crystallogr. Sect. D Biol. Crystallogr.* **54**, 905–921
- Jones, T. A., Zou, J. Y., Cowan, S. W., and Kjeldgaard, M. (1991) *Acta Crystallogr. Sect. D Biol. Crystallogr.* **47**, 110–119
- Laskowski, R. A., MacArthur, M. W., Moss, D. S., and Thornton, J. M. (1993) *J. Appl. Crystallogr.* **26**, 283–291
- Antonini, E. (1965) *Physiol. Rev.* **45**, 123–170
- Lad, L., Wang, J., Li, H., Friedman, J., Bhaskar, B., Ortiz de Montellano, P. R., and Poulos, T. L. (2003) *J. Mol. Biol.* **330**, 527–538
- Sugishima, M., Sakamoto, H., Higashimoto, Y., Noguchi, M., and Fukuyama, K. (2003) *J. Biol. Chem.* **278**, 32352–32358
- Lad, L., Friedman, J., Li, H., Bhaskar, B., Ortiz de Montellano, P. R., and Poulos, T. L. (2004) *Biochemistry* **43**, 3793–3801
- Lad, L., Ortiz de Montellano, P. R., and Poulos, T. L. (2004) *J. Inorg. Biochem.*, in press
- Ortiz de Montellano, P. R. (1998) *Acc. Chem. Res.* **31**, 543–549
- Davydov, R., Kofman, V., Fujii, H., Yoshida, T., Ikeda-Saito, M., and Hoffman, B. M. (2002) *J. Am. Chem. Soc.* **124**, 1798–1808
- Wilks, A., Torpey, J., and Ortiz de Montellano, P. R. (1994) *J. Biol. Chem.* **269**, 29553–29556
- Torpey, J., and Ortiz de Montellano, P. R. (1997) *J. Biol. Chem.* **272**, 22008–22014
- Liu, Y., Moenne-Loccoz, P., Loehr, T., and Ortiz de Montellano, P. R. (1997) *J. Biol. Chem.* **272**, 6909–6917
- Medforth, C. J., Senge, M. O., Smith, K. M., Sparks, L. D., and Shelnutz, J. A. (1992) *J. Am. Chem. Soc.* **114**, 9859–9869
- Barkigia, K. M., Berber, M. D., Fajer, J., Medforth, C. J., Renner, M. W., and Smith, K. M. (1990) *J. Am. Chem. Soc.* **112**, 8851–8857
- Senge, M., Ema, T., and Smith, K. (1995) *J. Chem. Soc. Chem. Commun.*

- 733–734
53. Li, Y., Syvitiski, R., Auclair, K., Wilks, A., Ortiz de Montellano, P. R., and La Mar, G. N. (2002) *J. Biol. Chem.* **277**, 33018–33031
54. Syvitiski, R. T., Li, Y., Auclair, K., Ortiz de Montellano, P. R., and La Mar, G. N. (2002) *J. Am. Chem. Soc.* **124**, 14296–14297
55. Hansch, C., Leo, A., and Hoekman, D. (1995) *Exploring QSAR: Hydrophobic, Electronic, and Steric Constants*, pp. 231–273 American Chemical Society, Washington, D. C.
56. Zhou, H., Migita, C. T., Sato, M., Sun, D., Zhang, X., Ikeda-Saito, M., Fujii, H., and Yoshida, T. (2000) *J. Am. Chem. Soc.* **122**, 8311–8312
57. Friedman, J., Lad, L., Li, H., Wilks, A., and Poulos, T. L. (2004) *Biochemistry* **43**, 5239–5245